Article

High Nuclearity Iridium–Platinum Clusters: Synthesis, Structures, Bonding, and Reactivity

Richard D. Adams, Burjor Captain, Michael B. Hall, Jack L. Smith,, and Charles Edwin Webster

J. Am. Chem. Soc., **2005**, 127 (3), 1007-1014• DOI: 10.1021/ja0443777 • Publication Date (Web): 31 December 2004

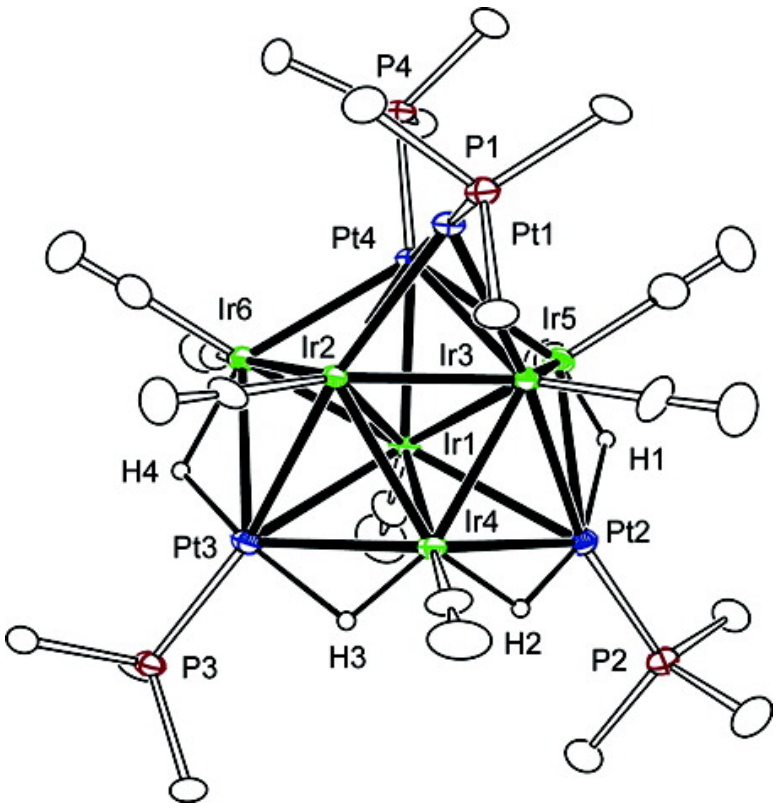

More About This Article

Additional resources and features associated with this article are available within the HTML version:

- Supporting Information
- Links to the 5 articles that cite this article, as of the time of this article download
- Access to high resolution figures
- Links to articles and content related to this article

J|A|C|S
ARTICLES
Published on Web 12/31/2004

High Nuclearity Iridium−Platinum Clusters: Synthesis, Structures, Bonding, and Reactivity

Richard D. Adams,*,† Burjor Captain,† Michael B. Hall,‡ Jack L. Smith, Jr.,† and Charles Edwin Webster‡

Contribution from the Department of Chemistry and Biochemistry and the USC Nanocenter, University of South Carolina, Columbia, South Carolina 29208, and Department of Chemistry, Texas A&M University, College Station, Texas 77843-3255

Received September 15, 2004; E-mail: Adams@mail.chem.sc.edu

Abstract: The reaction of $Ir_4(CO)_{12}$ with an excess of $Pt(PBu^t_3)_2$ at room temperature yielded the bis-$Pt(PBu^t_3)$ adduct $Ir_4(CO)_{12}[Pt(PBu^t_3)]_2$ (**9**), which contains two $Pt(PBu^t_3)$ groups bridging opposite edges of a central Ir_4 pseudotetrahedron. The same reaction at 110 °C yielded two new higher nuclearity complexes, $Ir_8(CO)_{12}[Pt(PBu^t_3)]_4$ (**10**) and $Ir_6(CO)_{10}[Pt(PBu^t_3)]_4$ (**11**). Compound **10** consists of a central $Ir_4(CO)_4$ tetrahedron with four edge-bridging $Ir(CO)_2$ groups and four $Pt(PBu^t_3)$ groups that are each bonded to Ir_3 triangles of the Ir_4 tetrahedron and two of the $Ir(CO)_2$ groups. Compound **11** consists of a central $Ir_4(CO)_4$ pseudotetrahedron with two edge-bridging $Ir(CO)_2$ groups and four $Pt(PBu^t_3)$ groups; one $Pt(PBu^t_3)$ group is bonded to five iridium atoms as found in **10**; two are bonded to four iridium atoms, and one is bonded to one of the outer Ir_2Pt triangles. Compound **11** reacted with hydrogen at 97 °C to give the new tetrahydrido complex $Ir_6(CO)_8[Pt(PBu^t_3)]_4(\mu\text{-H})_4$ (**12**). Compound **12** is formed by the loss of the two bridging carbonyl ligands from **11** and the addition of four hydrido ligands. All four new compounds were characterized by both ^1H and ^{31}P NMR and by single-crystal X-ray diffraction analyses. The bonding in **9** was studied by Fenske−Hall molecular orbital calculations, which in this case provides a delocalized bonding description for the Ir−Ir and Ir−Pt bonding, where the attachment of the 0 e^- fragments of $Pt(PR_3)$ use Ir−Ir bonding orbitals of the $Ir_4(CO)_{12}$ cluster to form multicenter Pt−Ir bonds.

Introduction

There is much current interest in the synthesis of bimetallic cluster complexes because of their use as precursors in the preparation of oxide-supported heterogeneous catalysts.[1] In his pioneering work on petroleum reforming catalysts, Sinfelt showed that when platinum was combined with iridium, a vastly superior catalyst was produced.[2] Today, bimetallic reforming catalysts are in widespread use industrially.[3] Bimetallic catalysts have an advantage over their monometallic counterparts both in higher activity and higher selectivity due to synergy between the different elements.[4] Thus, the preparation of platinum−containing bimetallic clusters has received considerable attention.[5]

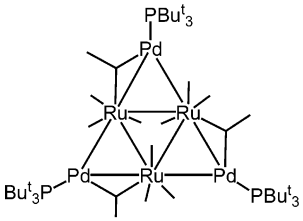

1

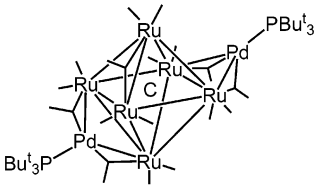

2

We have recently shown that the $M(PBu^t_3)_2$ compounds (M = Pt or Pd) readily react with metal carbonyl cluster complexes by adding $M(PBu^t_3)$ groups across metal−metal bonds.[6] For example, the $Pd(PBu^t_3)_2$ compound reacts with ruthenium carbonyl cluster complexes, such as $Ru_3(CO)_{12}$ and $Ru_6(CO)_{17}(\mu_6\text{-C})$, to form the Lewis acid−base adducts, $Ru_3(CO)_{12}[Pd(PBu^t_3)]_3$ (**1**) and $Ru_6(CO)_{17}(\mu_6\text{-C})[Pd(PBu^t_3)]_2$ (**2**), respectively.[6a] The $Ru_5(CO)_{15}(\mu_5\text{-C})$ complex also reacts with $M(PBu^t_3)_2$ (M = Pt or Pd), yielding the $Ru_5(CO)_{15}(C)[M(PBu^t_3)]$ (**3**) and $Ru_5(CO)_{15}(\mu_6\text{-C})[Pd(PBu^t_3)]_2$ (**4**) adducts.[6b,c] Compound **3** exists in

† University of South Carolina.
‡ Texas A&M University.

(1) Thomas, J. M.; Johnson, B. F. G.; Raja, R.; Sankar, G.; Midgley, P. A. *Acc. Chem. Res.* **2003**, *36*, 20. (b) Raja, R.; Khimyak, T.; Thomas, J. M.; Hermans, S.; Johnson, B. F. G. *Angew. Chem., Int. Ed.* **2001**, *40*, 4638. (c) Hermans, S.; Raja, R.; Thomas, J. M.; Johnson, B. F. G.; Sankar, G.; Gleeson, D. *Angew. Chem., Int. Ed.* **2001**, *40*, 1211. (d) Shephard, D. S.; Maschmeyer, T.; Johnson, B. F. G.; Thomas, J. M.; Sankar, G.; Ozkaya, D.; Zhou, W.; Oldroyd, R. D.; Bell, R. G. *Angew. Chem., Int. Ed. Engl.* **1997**, *36*, 2242. (e) Shephard, D. S.; Maschmeyer, T.; Sankar, G.; Thomas, J. M.; Ozkaya, D.; Johnson, B. F. G.; Raja, R.; Oldroyd, R. D.; Bell, R. G. *Chem.—Eur. J.* **1998**, *4*, 12.
(2) Sinfelt, J. H. *Bimetallic Catalysts: Discoveries, Concepts and Applications*; Wiley: New York, 1983. (b) Sinfelt, J. H. *Sci. Am.* **1985**, *253*, 90. (c) Sinfelt, J. H.; Via, G. H. *J. Catal.* **1979**, *56*, 1.
(3) Xiao, J.; Puddephatt, R. J. *Coord. Chem. Rev.* **1995**, *143*, 457. (b) Dees, M. J.; Ponec, V. *J. Catal.* **1989**, *115*, 347. (c) Rice, R. W.; Lu, K. *J. Catal.* **1982**, *77*, 104. (d) Rasser, J. C.; Beindorff, W. H.; Scholten, J. F. *J. Catal.* **1979**, *59*, 211.
(4) Raja, R.; Sankar, G.; Hermans, S.; Shephard, D. S.; Bromley, S.; Thomas, J. M.; Johnson, B. F. G. *Chem. Commun.* **1999**, 1571. (b) Alexeev, O. S.; Gates, B. C. *Ind. Eng. Chem. Res.* **2003**, *42*, 1571. (c) Goodman, D. W.; Houston, J. E. *Science* **1987**, *236*, 403. (d) Ichikawa, M. *Adv. Catal.* **1992**, *38*, 283.
(5) Farrugia, L. J. *Adv. Organomet. Chem.* **1990**, *31*, 301. (b) Pignolet, L. H.; Aubart, M. A.; Craighead, K. L.; Gould, R. A. T.; Krogstad, D. A.; Wiley, J. S. *Coord. Chem. Rev.* **1995**, *143*, 219.

solution as two isomers, **3a** and **3b**, that interconvert rapidly on the NMR time scale.

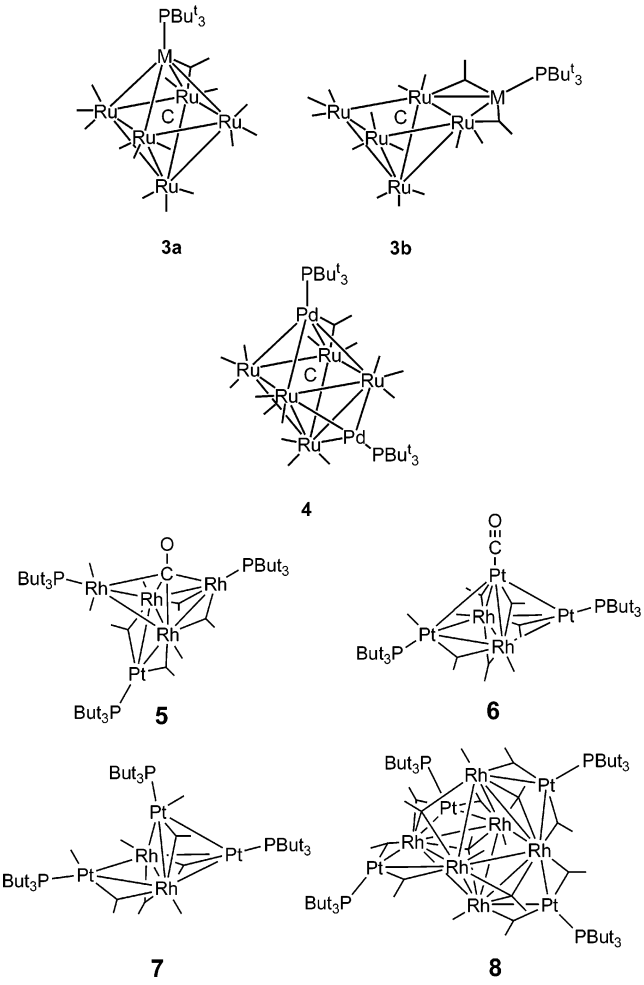

We have also prepared several rhodium−platinum cluster complexes by the reaction of $Rh_4(CO)_{12}$ with $Pt(PBu^t_3)_2$.[6d] Four new products, $Rh_4(CO)_4(\mu\text{-}CO)_4(\mu_4\text{-}CO)(PBu^t_3)_2[Pt(PBu^t_3)]$ (**5**), $Rh_2(CO)_8[Pt(PBu^t_3)]_2[Pt(CO)]$ (**6**), $Rh_2(CO)_8[Pt(PBu^t_3)]_3$ (**7**), and $Rh_6(CO)_{16}[Pt(PBu^t_3)]_4$ (**8**), were obtained. Interestingly, all four compounds show evidence of some type of fluxional behavior, involving either the ligands or the metal atoms themselves. Compound **7**, for example, undergoes a dynamical rearrangement of the metal atoms that averages the three nonequivalent platinum phosphine groups.

There have been very few reports of high nuclearity platinum−iridium cluster complexes.[7] Herein, we describe some of the largest platinum−iridium cluster complexes reported to date. They were obtained from reactions of $Pt(PBu^t_3)_2$ with $Ir_4(CO)_{12}$. We also describe an example of hydrogen activation by one of these complexes. Three new compounds, $Ir_4(CO)_{12}[PtP(Bu^t_3)]_2$ (**9**), $Ir_8(CO)_{12}[PtP(Bu^t_3)]_4$ (**10**), and $Ir_6(CO)_{10}[PtP(Bu^t_3)]_4$ (**11**), and a hydride containing a derivative of **11**, $Ir_6(CO)_8[PtP(Bu^t_3)]_4(\mu\text{-}H)_4$ (**12**), were isolated and structurally characterized.

Experimental Section

General Data. All of the reactions were performed under a nitrogen atmosphere. Reagent grade solvents were dried by the standard procedures and were freshly distilled prior to use. Infrared spectra were recorded on a Thermo-Nicolet Avatar 360 FT-IR spectrophotometer. ^{1}H NMR spectra were recorded on a Varian Mercury 400 and Varian Inova 500 spectrometer operating at 400.1 and 500.2 MHz, respectively. ^{31}P{^{1}H} NMR spectra were recorded on a Varian Mercury 400 spectrometer operating at 162.0 MHz and were externally referenced against 85% *ortho*-H_3PO_4. Elemental analyses were performed by Desert Analytics (Tucson, AZ). Product separations were performed by TLC in air on Analtech 0.5 mm silica gel 60 Å F_{254} glass plates. Tetrairidium dodecacarbonyl, $Ir_4(CO)_{12}$, and bis(tri-*tert*-butyl phosphine)platinum(0), $Pt(PBu^t_3)_2$, were obtained from Strem and were used without further purification.

Reaction of $Ir_4(CO)_{12}$ with $Pt(PBu^t_3)_2$ at 25 °C. $Pt(PBu^t_3)_2$ (50.0 mg, 0.084 mmol) was added to a suspension of $Ir_4(CO)_{12}$ (30.0 mg, 0.027 mmol) in 100 mL of CH_2Cl_2. The reaction mixture was stirred at room temperature for 8 h. The solvent was removed in vacuo, and the product was separated by TLC using a 2:1 hexane/methylene chloride solvent mixture to yield 25.8 mg (50%) of brown $Ir_4(CO)_{12}[Pt(PBu^t_3)]_2$ (**9**). Spectral data for **9**: IR ν_{CO} (cm^{-1} in CH_2Cl_2) ν 2064 (m), 2037 (vs), 2004 (m), 1854 (w), 1816 (w); ^{1}H NMR ($CDCl_3$ in ppm) δ 1.46 (d, 54 H, CH_3, $^3J_{P-H}$ = 13 Hz); ^{31}P{^{1}H} NMR ($CDCl_3$ in ppm) δ 129.0 (s, 2 P, $^1J_{Pt-P}$ = 5851 Hz). Anal. Calcd: C, 25.45; H, 3.05. Found: C, 25.36; H, 2.66.

Reaction of $Ir_4(CO)_{12}$ with $Pt(PBu^t_3)_2$ at 110 °C. $Ir_4(CO)_{12}$ (30.0 mg, 0.027 mmol) was suspended in 100 mL of toluene and heated to reflux. $Pt(PBu^t_3)_2$ (50.0 mg, 0.084 mmol) was added, and the color of the solution immediately changed from yellow to dark brown. The reaction mixture was stirred for 5 h at reflux. The solvent was removed in vacuo, and the products were separated by TLC using a 2:1 hexane/methylene chloride solvent mixture to yield in order of elution 7.4 mg (16%) of brown $Ir_8(CO)_{12}[Pt(PBu^t_3)]_4$ (**10**) and 17.8 mg (33%) of green $Ir_6(CO)_{10}[Pt(PBu^t_3)]_4$ (**11**). Spectral data for **10**: IR ν_{CO} (cm^{-1} in CH_2Cl_2) ν 2000 (s), 1971 (m), 1958 (w); ^{1}H NMR ($CDCl_3$ in ppm) δ 1.38 (d, 108 H, CH_3, $^3J_{P-H}$ = 13 Hz); ^{31}P{^{1}H} NMR ($CDCl_3$ in ppm) δ 92.5 (s, 4 P, $^1J_{Pt-P}$ = 4248 Hz). Anal. Calcd: C, 20.81; H, 3.14. Found: C, 20.71; H, 2.88. Spectral data for **11**: IR ν_{CO} (cm^{-1} in hexane) ν 2014(w), 1995 (vs), 1986 (s), 1961 (s), 1955 (m), 1945 (m), 1934(w), 1928 (w), 1782 (w), 1760 (w); ^{1}H NMR at 25 °C (toluene-d_8 in ppm) δ 1.81 (br), 1.61 (d, 54 H, CH_3, $^3J_{P-H}$ = 13 Hz), 0.93 (d, 27 H, CH_3, $^3J_{P-H}$ = 13 Hz); ^{1}H NMR at 100 °C (toluene-d_8 in ppm) δ 1.78 (d, 27 H, CH_3, $^3J_{P-H}$ = 13 Hz), 1.61 (d, 54 H, CH_3, $^3J_{P-H}$ = 13 Hz), 0.99 (d, 27 H, CH_3, $^3J_{P-H}$ = 13 Hz); ^{31}P{^{1}H} NMR (toluene-d_8 in ppm) δ 131.8 (s, 1 P, $^1J_{Pt-P}$ = 3871 Hz), 91.2 (s, 2 P, $^1J_{Pt-P}$ = 5287 Hz), 75.263 (s, 1 P, $^1J_{Pt-P}$ = 4326 Hz, $^3J_{Pt-P}$ = 627 Hz). Anal. Calcd: C, 23.52; H, 3.65. Found: C, 23.54; H, 3.30.

Reaction of 11 with Hydrogen. A solution of **11** (10.0 mg, 0.0033 mmol) in heptane was heated to reflux under a slow purge of hydrogen for 3 h. The solvent was removed in vacuo, and the product was separated by TLC using a 2:1 hexane/methylene chloride solvent mixture to yield 4.5 mg (45%) of green $Ir_6(CO)_8[Pt(PBu^t_3)]_4(\mu\text{-}H)_4$, **12**. Spectral data for **12**: IR ν_{CO} (cm^{-1} in hexane) ν 2025 (m), 2008 (s), 1968 (s), 1956 (s), 1940 (m), 1930 (m); ^{1}H NMR at 25 °C (toluene-d_8 in ppm) δ 1.86 (br), 1.53 (d, 54 H, CH_3, $^3J_{P-H}$ = 13 Hz), 0.88 (d, 27 H, CH_3, $^3J_{P-H}$ = 13 Hz), −10.57 (s, 2 H, $^1J_{Pt-H}$ = 706 Hz), −15.39 (s, 2 H, $^1J_{Pt-H}$ = 776 Hz); ^{1}H NMR of hydride region at −50 °C (toluene-d_8 in ppm) δ −10.30 (d, 2 H, $^1J_{Pt-H}$ = 709 Hz, $^2J_{P-H}$ = 39 Hz), −14.98

(6) Adams, R. D.; Captain, B.; Fu, W.; Smith, M. D. *J. Am. Chem. Soc.* **2002**, *124*, 5628. (b) Adams, R. D.; Captain, B.; Fu, W.; Pellechia, P. J.; Smith, M. D. *Angew. Chem., Int. Ed.* **2002**, *41*, 1951. (c) Adams, R. D.; Captain, B.; Fu, W.; Pellechia, P. J.; Smith, M. D. *Inorg. Chem.* **2003**, *42*, 2094. (d) Adams, R. D.; Captain, B.; Pellechia, P. J.; Smith, J. L. *Inorg. Chem.* **2004**, *43*, 2695. (e) Adams, R. D.; Captain, B.; Fu, W.; Smith, J. L.; Smith, M. D. *Organometallics* **2004**, *23*, 589. (f) Adams, R. D.; Captain, B.; Fu, W.; Hall, M. B.; Smith, M. D.; Webster, C. E. *Inorg. Chem.* **2004**, *43*, 3921. (g) Adams, R. D.; Captain, B.; Smith, M. D. *J. Cluster Sci.* **2004**, *15*, 139. (h) Adams, R. D.; Captain, B.; Fu, W.; Smith, M. D. *J. Organomet. Chem.* **2003**, *682*, 113.

(7) Sterenberg, B. T.; Jenkins, H. A.; Puddephatt, R. J. *Organometallics* **1999**, *18*, 219. (b) Araujo, M. H.; Avent, A. G.; Hitchcock, P. B.; Nixon, J. F.; Vargas, M. D. *Organometallics* **1998**, *17*, 5460. (c) Bhaduri, S.; Sharma, K. R.; Clegg, W.; Sheldrich, G. M.; Stakle, D. *J. Chem. Soc., Dalton Trans.* **1984**, *12*, 2851. (d) Freeman, M. J.; Miles, A. D.; Murray, M.; Orpen, A. G.; Stone, G. A. *Polyhedron* **1984**, *3*, 1093.

Table 1. Crystallographic Data for Compounds **9** and **10**

compound	**9**	**10**
empirical formula	$Ir_4Pt_2P_2O_{12}C_{36}H_{54}\cdot C_8H_{10}$	$Ir_8Pt_4P_4O_{12}C_{60}H_{108}$
formula weight	2005.87	3463.30
crystal system	triclinic	orthorhombic
lattice parameters		
a (Å)	8.6678(11)	41.4988(13)
b (Å)	14.6290(18)	27.0640(9)
c (Å)	22.004(3)	25.7975(8)
α (deg)	101.230(2)	90
β (deg)	94.949(2)	90
γ (deg)	91.420(2)	90
V (Å^3)	2724.1(6)	28973.8(16)
space group	$P\bar{1}$	*Pbcn*
Z value	2	12
ρ_{calc} (g cm^{-3})	2.445	2.382
μ (Mo Kα) (mm^{-1})	14.96	16.848
temperature (K)	296(2)	296(2)
$2\Theta_{max}$ (deg)	50.06	48.02
No. of observations	7296	17602
No. of parameters	555	1190
goodness of fit	1.061	0.937
maximum shift in cycle	0.003	0.009
residuals[a] R_1; wR_2 ($I > 2\sigma(I)$)	0.0562; 0.1439	0.0409; 0.0962
absorption correction	SADABS	SADABS
max/min	1.000/0.615	1.000/0.268
largest peak in final diff. map (e Å^{-3})	4.033	1.683

Table 2. Crystallographic Data for Compounds **11** and **12**

compound	**11**	**12**
empirical formula	$Ir_6Pt_4P_4O_{10}C_{58}H_{108}\cdot CH_3CN$	$Ir_6Pt_4P_4O_8C_{56}H_{108}$
formula weight	3063.94	2966.86
crystal system	monoclinic	triclinic
lattice parameters		
a (Å)	19.6831(6)	12.5080(7)
b (Å)	15.6634(4)	14.9767(9)
c (Å)	25.1088(7)	23.6748(14)
α (deg)	90	105.119(1)
β (deg)	91.732(1)	99.902(1)
γ (deg)	90	104.222(1)
V (Å^3)	7737.6(4)	4016.0(4)
space group	$P2_1/n$	$P\bar{1}$
Z value	4	2
ρ_{calc} (g cm^{-3})	2.630	2.579
μ (Mo Kα) (mm^{-1})	17.605	16.961
temperature (K)	296(2)	100(2)
$2\Theta_{max}$ (deg)	52.04	54.34
No. of observations	11053	16256
No. of parameters	766	849
goodness of fit	0.992	1.062
maximum shift in cycle	0.009	0.003
residuals[a] R_1; wR_2 ($I > 2\sigma(I)$)	0.0439; 0.0896	0.0299; 0.0727
absorption correction	SADABS	SADABS
max/min	1.000/0.199	1.000/0.230
largest peak in final diff. map (e Å^{-3})	3.957	2.801

[a] $R = \sum_{hkl}(||F_{obs}| - |F_{calc}||)/\sum_{hkl}|F_{obs}|$; $R_w = [\sum_{hkl}w(|F_{obs}| - |F_{calc}|)^2/\sum_{hkl}wF^2_{obs}]^{1/2}$; $w = 1/\sigma^2(F_{obs})$; GOF $= [\sum_{hkl}w(|F_{obs}| - |F_{calc}|)^2/(n_{data} - n_{vari})]^{1/2}$.

(d, 2 H, $^1J_{Pt-H} = 763$ Hz, $^2J_{P-H} = 7$ Hz); ^{1}H NMR at 100 °C (toluene-d_8 in ppm) δ 1.95 (d, 27 H, CH_3, $^3J_{P-H} = 11$ Hz), 1.57 (d, 54 H, CH_3, $^3J_{P-H} = 13$ Hz), 0.94 (d, 27 H, CH_3, $^3J_{P-H} = 123$ Hz), −10.77 (s, br, 2 H), −15.74 (s, br, 2 H); ^{31}P{^{1}H} NMR at 25 °C (toluene-d_8 in ppm) δ 129.8 (s, 1 P, $^1J_{Pt-P} = 3754$ Hz), 90.5 (s, 2 P, $^1J_{Pt-P} = 4758$ Hz), 61.2 (s, 1 P, $^1J_{Pt-P} = 6670$ Hz, $^3J_{Pt-P} = 621$ Hz). Anal. Calcd: C, 23.11; H, 3.38. Found: C, 23.22; H, 3.36. MS (ES): *m*/*z* 2971 M^+.

Crystallographic Analyses. Dark-brown single crystals of **9** suitable for X-ray diffraction analysis were obtained by slow evaporation of solvent from a solution of *p*-xylene at room temperature. Dark-brown single crystals of **10** were obtained by slow evaporation of a benzene/octane solvent mixture at 8 °C. Dark-green single crystals of **11** were obtained by slow evaporation of a methylene chloride/acetonitrile solvent mixture at 8 °C. Dark-green single crystals of **12** were obtained by slow evaporation of solvent from a solution of diethyl ether at −18 °C. Each data crystal was glued onto the end of a thin glass fiber. X-ray intensity data were measured by using a Bruker SMART APEX CCD-based diffractometer using Mo Kα radiation ($\lambda = 0.71073$ Å). The raw data frames were integrated with the SAINT+ program[8] by using a narrow-frame integration algorithm. Corrections for Lorentz and polarization effects were also applied with SAINT+. An empirical absorption correction based on the multiple measurement of equivalent reflections was applied using the SADABS program. All structures were solved by a combination of direct methods and difference Fourier syntheses and refined by full-matrix least-squares on F^2 using the SHELXTL software package.[9] All non-hydrogen atoms were refined with anisotropic thermal parameters. All *tert*-butyl hydrogen atoms were placed in geometrically idealized positions and included as standard riding atoms during the least-squares refinements. Crystal data, data collection parameters, and results of the analyses are listed in Tables 1 and 2. Data for **9**−**12** were collected at 296(2) K, and data for **12** were collected at 100(2) K.

Compounds **9** and **12** crystallized in the triclinic crystal system. For both compounds, the $P\bar{1}$ space group was assumed and confirmed by the successful solution and refinement of the structures. One molecule of *p*-xylene from the crystallization solvent co-crystallized with **9** and was located and refined with isotropic displacement parameters. Two molecules of diethyl ether co-crystallized with **12** and were located and refined with anisotropic thermal parameters. All four hydride ligands were located and successfully refined with one geometric restraint.

Compound **10** crystallized in the orthorhombic crystal system. The *Pbcn* space group was established on the basis of the systematic absences observed during the collection of the intensity data. There are two independent molecules of **10** in the asymmetric unit, one that is ordered in a general position and one that lies on a mirror plane, thus generating 12 formula equivalents per unit cell. The packing of the molecules generates large cavities that are filled with disordered solvent molecules of crystallization. No reasonable disorder model could be obtained for these species, and therefore they were accounted for with the SQUEEZE/PLATON program.[10] Two crystallographically nonequivalent cavities of equal volume are present at (0, 0.500, 0.244) and (0, 0.500, 0.775). The program calculated a total solvent-accessible volume per unit cell of 7467.2 Å^3, or 25.8% of the total unit cell volume, corresponding to 4348 e$^-$/cell. The contribution of these diffusely scattering species was removed from the structure factor calculations. The tabulated $F(000)$, M_w, and density reflect the known unit cell contents only.

Compound **11** crystallized in the monoclinic crystal system. The $P2_1/n$ space group was identified uniquely on the basis of the systematic absences in the intensity data. One molecule of CH_3CN from the crystallization solvent co-crystallized with **11** and was located and refined with anisotropic thermal parameters.

Molecular Orbital Calculations. All molecular orbital calculations reported here are from the Fenske−Hall method.[11] Fenske−Hall

(8) *SAINT+*, version 6.2a; Bruker Analytical X-ray Systems, Inc.: Madison, WI, 2001.
(9) Sheldrick, G. M. *SHELXTL*, version 6.1; Bruker Analytical X-ray Systems, Inc.: Madison, WI, 1997.
(10) Spek, A. L. *PLATON: A Multipurpose Crystallographic Tool*; Utrecht University: Utrecht, The Netherlands, 1998.
(11) Hall, M. B.; Fenske, R. F. *Inorg. Chem.* **1972**, *11*, 768−775.

Scheme 1

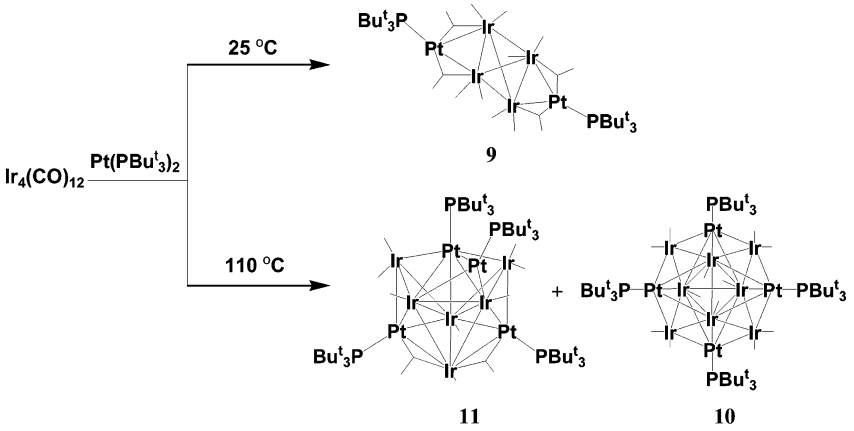

calculations were performed utilizing a graphical user interface developed[12] to build inputs and view outputs from stand-alone Fenske−Hall (version 5.2) and MOPLOT2[13] binary executables. Contracted double-ζ basis sets were used for the Ir and Pt 5d, P 3p, and C and O 2p atomic orbitals. PH_3 was used in place of PBu^t_3 in these calculations. The Fenske−Hall scheme is a nonempirical approximate method that is capable of calculating molecular orbitals for very large transition metal systems and has built-in fragment analysis routines that allow one to assemble transition metal cluster structures from the ligand containing fragments.

Results and Discussion

The reaction of $Ir_4(CO)_{12}$ with an excess of $Pt(PBu^t_3)_2$ at room temperature gave the new compound, $Ir_4(CO)_{12}[Pt(PBu^t_3)]_2$ (**9**), in 50% yield. However, at 110 °C, the same reaction gave two new higher nuclearity compounds, $Ir_8(CO)_{12}[Pt(PBu^t_3)]_4$ (**10**) and $Ir_6(CO)_{10}[Pt(PBu^t_3)]_4$ (**11**), in 16 and 33% yields, respectively (Scheme 1). Interestingly, it was not possible to convert **9** into **10** or **11** at the same temperature at which they were formed in the original reaction. All three compounds were characterized by a combination of IR, ^1H and ^{31}P NMR, single-crystal X-ray diffraction, and elemental analysis.

An ORTEP diagram of the molecular structure of **9** is shown in Figure 1. Selected intramolecular distances and angles for **9** are listed in Table 3. The structure of **9** consists of a central Ir_4 pseudotetrahedron. Two of the Ir−Ir bonds on opposite sides of the Ir_4 cluster contain bridging $Pt(PBu^t_3)$ groups. Each iridium atom contains two linear terminal carbonyl ligands, and each Ir−Pt bond has one bridging carbonyl ligand. Overall, the molecular structure has C_2 symmetry. The compound can be viewed a bis-$Pt(PBu^t_3)$ adduct of $Ir_4(CO)_{12}$ because no CO ligands were lost during the course of the reaction and, therefore, can be constructed from an $Ir_4(CO)_{12}$ fragment and two $Pt(PR_3)$ fragments. The Ir−Ir bonds bridged by the $Pt(PR_3)$ groups [Ir(1)−Ir(4) = 2.7462(9) Å and Ir(2)−Ir(3) = 2.7486(9) Å] are significantly longer than the unbridged Ir−Ir bonds that lie in the range of 2.7010(9)−2.7260(9) Å. This can be explained by delocalization of the electrons in these Ir−Ir-bridged bonds to the platinum atom; see below. For the Ir−Ir bond distances in $Ir_4(CO)_{12}$, the average Ir−Ir distance = 2.693 Å.[14] The $^{31}P\{^1H\}$ NMR spectrum of **9** shows only one resonance at 129.0 ppm with appropriate one-bond coupling to platinum ($^1J_{Pt-P}$ = 5851 Hz), indicating that the phosphine ligands are indeed directly bonded to platinum as assigned in the structure determinations, and also that two platinum phosphine groups are equivalent.

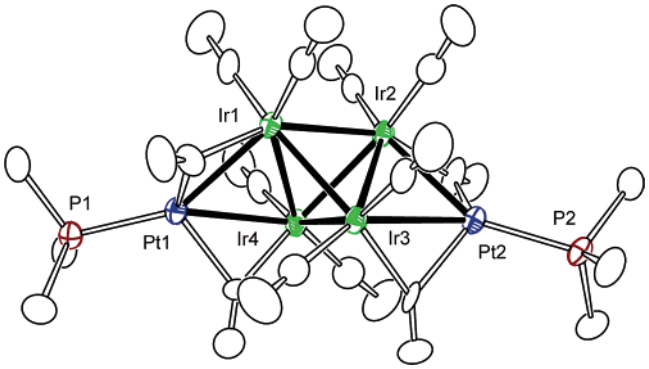

Figure 1. ORTEP diagram of the molecular structure of $Ir_4(CO)_{12}[Pt(PBu^t_3)]_2$ (**9**) showing 40% thermal ellipsoid probabilities. The methyl groups on the *tert*-butyl groups have been omitted for clarity.

Table 3. Selected Intramolecular Distances and Angles for Compounds **9** and **10**[a]

9		**10**	
Bond Distances (Å)			
Ir(1)−Ir(2)	2.7109(8)	Ir(1)−Ir(1)*	2.7328(8)
Ir(1)−Ir(3)	2.7010(9)	Ir(1)−Ir(3)	2.6421(7)
Ir(1)−Ir(4)	2.7462(9)	Ir(2)−Ir(1)*	2.7303(6)
Ir(2)−Ir(3)	2.7486(9)	Ir(2)−Ir(3)	2.6342(6)
Ir(2)−Ir(4)	2.7014(9)	Pt(1)−Ir(1)	2.6608(6)
Ir(3)−Ir(4)	2.7262(9)	Pt(1)−Ir(1)*	2.8958(6)
Pt(1)−Ir(1)	2.7591(9)	Pt(1)−Ir(2)	2.9151(6)
Pt(1)−Ir(4)	2.7535(9)	Pt(1)−Ir(3)	2.6820(6)
Pt(2)−Ir(2)	2.7527(9)	Pt(1)−Ir(5)	2.6717(6)
Pt(2)−Ir(3)	2.7472(9)	C−O (av)	1.13(1)
C−O (av)	1.19(2)		
Bond Angles (deg)			
Ir(1)−Ir(2)−Ir(3)	59.30(2)	Ir(1)−Ir(2)−Ir(1)*	60.35(2)
Ir(1)−Ir(2)−Ir(4)	60.98(2)	Ir(1)−Ir(3)−Ir(2)	62.21(2)
Ir(1)−Pt(1)−Ir(4)	59.76(2)	Ir(1)−Pt(1)−Ir(1)*	58.76(2)
Ir(2)−Ir(1)−Pt(1)	119.02(3)	Ir(3)−Ir(1)−Ir(5)	118.30(2)
Ir(3)−Ir(1)−Pt(1)	93.66(3)	Ir(3)−Pt(1)−Ir(5)	116.18(2)
Ir(4)−Ir(3)−Pt(2)	92.54(3)	Pt(1)−Ir(3)−Pt(2)*	114.53(2)

[a] Estimated standard deviations in the least significant figure are given in parentheses.

Molecular Orbital Calculations for 9. One can envision the $Ir_4(CO)_{12}[Pt(PR_3)]_2$ cluster being assembled from four

(12) Manson, J.; Webster, C. E.; Hall, M. B. *JIMP*, Development Version 0.1.115 (built for Windows PC and Redhat Linux); Department of Chemistry, Texas A&M University: College Station, TX (http://www.chem.tamu.edu/jimp/, April 2004).

(13) Lichtenberger, D. L. *MOPLOT2*, version 2.0 (for orbital and density plots from linear combinations of Slater or Gaussian type orbitals); Department of Chemistry, University of Arizona: Tucson, AZ, June 1993.

(14) Churchill, M. R.; Hutchinson, J. P. *Inorg. Chem.* **1978**, *17*, 3528.

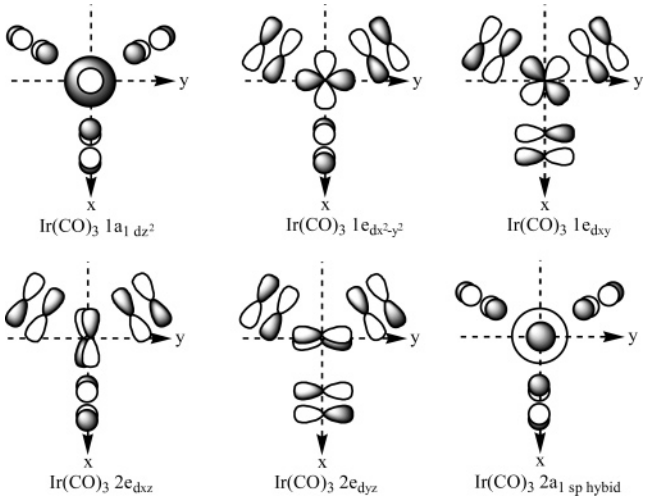

Figure 2. Illustration of the Ir "5d"- and "6s"-fragment orbitals and their CO π^* contributions. Because of the low symmetry, the **2e** (e_g) metal orbital, which would be σ^* with respect to the Ir←CO dative bond in O_h symmetry, mix with low-lying **e** symmetric π^* orbitals of the COs.

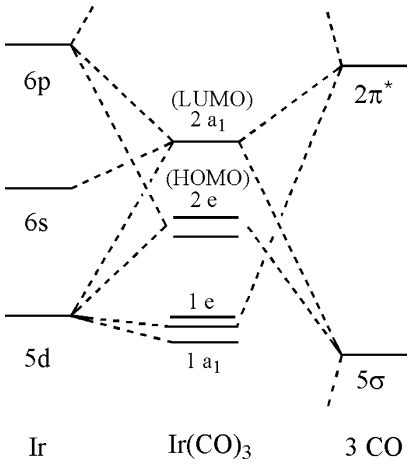

Figure 3. Molecular orbital diagram for the $Ir(CO)_3$ fragment.

$Ir(CO)_3$ fragments (Figures 2 and 3) and two $PtPR_3$ fragments (Figure 4; this cluster possesses C_2 symmetry, and the discussion of its bonding interactions will be based on this point group). As expected for the pseudo-octahedral $Ir(CO)_3$ fragment, the MO splitting shows three low-lying occupied orbitals from the pseudo-octahedral "t_{2g}" set (**1a$_1$** and **1e**) and two higher-lying orbitals (**2e**) from the "e_g" set with three electrons. The next lowest-lying orbital is the **2a$_1$**. The key orbitals of the $Pt(PR_3)$ fragment are the occupied **2e**, **1e**, and d_{z^2}-like **1a$_1$** HOMO and the "sp"-like **2a$_1$** LUMO. The combination of four $Ir(CO)_3$ fragments produces the C_2 symmetric $Ir_4(CO)_{12}$ core of the cluster (Figure 5). In this pseudotetrahedral core, the four t_{2g}-like sets produce 12 linear combinations, **1a**−**6a** and **1b**−**6b**, which are occupied Ir−CO π bonding (but cluster nonbonding). The four sets of e_g-like orbitals produce eight linear combinations, **7a**−**9a**, **11a**, and **7b**−**10b**. Of these, the six lowest-energy orbitals are occupied as cluster-bonding and nonbonding orbitals, while three high-lying antibonding orbitals are unoccupied. The **2a$_1$** orbitals combine and produce four orbitals, **10a** (the $Ir_4(CO)_{12}$ fragment HOMO) and three unoccupied orbitals (**12a**, **11b**, and **12b**).

The six principal metal−metal bonding orbitals for the $Ir_4(CO)_{12}$ portion of the molecule are shown on the left side of the energy level diagram (Figure 6), with symmetry labels derived from the C_2 symmetry of product **9**. Molecular orbital plots of these six orbitals are shown in Figure 7. These orbitals interact with two pairs of orbitals derived from symmetric and antisymmetric combinations of the d_{z^2}-like HOMO (**1a**, **1b**) and an sp-hybridized LUMO (**2a**, **2b**) derived from the $[Pt(PBu^t_3)]_2$ unit. These are shown on the right side of Figure 6. The combination of the $Ir_4(CO)_{12}$ core fragment orbitals with the $[Pt(PBu^t_3)]_2$ fragment orbitals results in cluster bonding MOs, as shown in the center of Figure 6. The best orbital overlap between these two last fragments is seen in the **2b** and **2a** cluster orbitals. In **2b**, the bonding interaction is mainly between the occupied **8b** orbital in the $Ir_4(CO)_{12}$ fragment, and the unoccupied antisymmetric sp hybrid (LUMO), **2b**, from the $[Pt(PBu^t_3)]_2$ fragments. This **2b** cluster orbital involves two symmetric three-center interactions, one across each of the two Ir_2Pt triangles (Figure 8). Appropriately, the symmetric sp hybrid (LUMO+1), **2a**, from the $[Pt(PBu^t_3)]_2$ fragments accepts electrons from the **7a** and **8a** orbitals of the $Ir_4(CO)_{12}$ fragment to generate the **2a** cluster orbital, as shown in Figure 9. Six other cluster orbitals (**1a**, **1b**, **3a**, **3b**, **4a**, and **5a**) are involved in Ir−Ir bonding in the Ir_4 core. The HOMO for this cluster is the **5a** orbital, which was derived from the Ir_4-bonding HOMO, the **10a** orbital in the $Ir_4(CO)_{12}$ fragment; this orbital is directed to the center of the Ir_4 core and has no significant interactions with the platinum atoms.

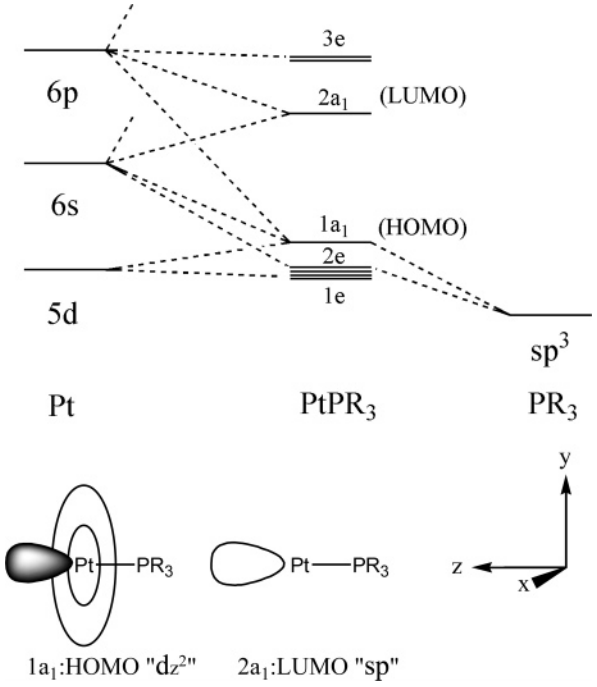

Figure 4. Molecular orbital diagram for the $PtPR_3$ fragment.

Higher Nuclearity Clusters Produced at Elevated Temperatures. An ORTEP diagram of the molecular structure of **10** is shown in Figure 10. Selected intramolecular distances and angles for **10** are listed in Table 3. The structure of **10** consists of a central tetrahedral $Ir_4(CO)_4$ core. There are four $Ir(CO)_2$ groups bridging four of the six edges of the $Ir_4(CO)_4$ core. There are also four $Pt(PBu^t_3)$ groups, and each Pt atom is bonded to five iridium atoms, which includes three from a triangular group of the central $Ir_4(CO)_4$ group and two of the edge-bridging $Ir(CO)_2$ groups. The molecule has a crystallographically imposed C_2 symmetry. The C_2 axis passes through the Ir(4) and Ir(5)

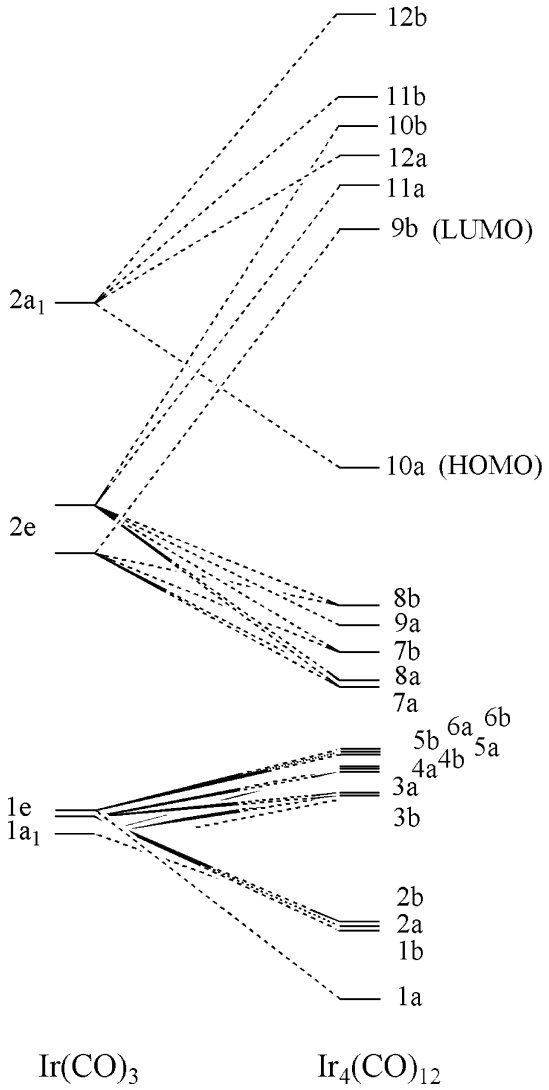

Figure 5. Molecular orbital diagram for the $Ir_4(CO)_{12}$ fragment under C_2 symmetry.

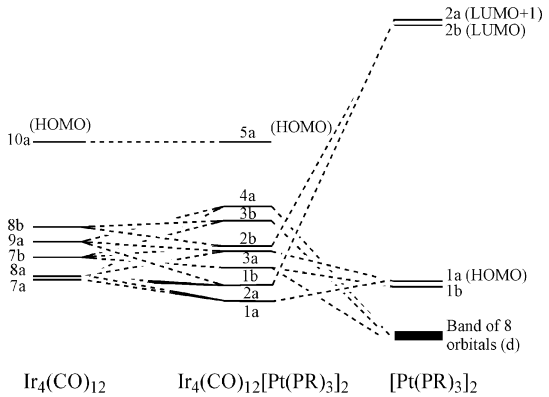

Figure 6. Molecular orbital diagram for the model cluster $Ir_4(CO)_{12}[Pt(PR_3)]_2$, R = H.

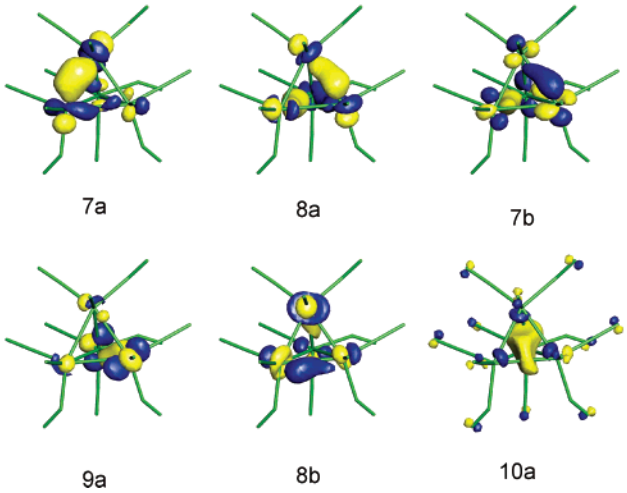

Figure 7. Molecular orbitals responsible for the bonding interactions in the $Ir_4(CO)_{12}$ unit (**7a**, **8a**, **7b**, **9a**, **8b**, and **10a**).

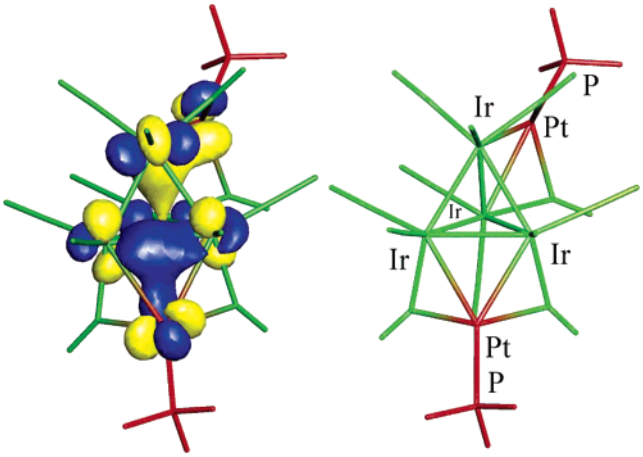

Figure 8. The **2b** orbital of the $Ir_4(CO)_{12}[Pt(PR_3)]_2$ cluster showing the interaction of the antisymmetric combination of the two Pt fragment LUMO orbitals with the **8b** orbital of the $Ir_4(CO)_{12}$ fragment.

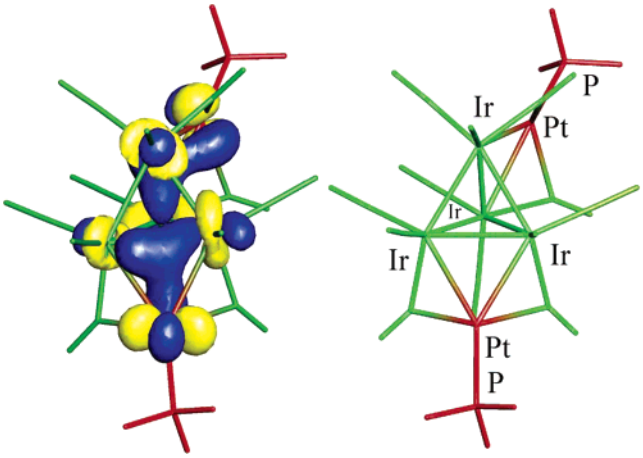

Figure 9. The **2a** orbital of the $Ir_4(CO)_{12}[Pt(PR_3)]_2$ cluster showing the interaction of the symmetric combination of the two Pt fragment LUMO+1 orbitals with the **7a** and **8a** orbitals of the $Ir_4(CO)_{12}$ fragment.

atoms. The Ir−Ir bond distances of the central Ir_4 tetrahedron all lie in the range of 2.7061(6)−2.7328(8) Å and are very similar to those observed in **9**. By contrast, the Ir−Ir bond distances between the iridium atoms in the interior tetrahedron and the outer iridium atoms are significantly shorter, 2.6342(6)−2.6513(6) Å. The platinum atoms are not symmetrically bonded to the five iridium atoms. For example, Pt(1) is pushed toward Ir(1) such that the distances of Pt(1)−Ir(1)* = 2.8958(6) Å and Pt(1)−Ir(2) = 2.9151(6) Å are much longer than the distance of Pt(1)−Ir(1) = 2.6597(6) Å. This shortening is probably due to steric interactions between the bulky tri-*tert*-butyl phosphine and the carbonyl ligands. As with **9**, the ^{31}P NMR spectrum of

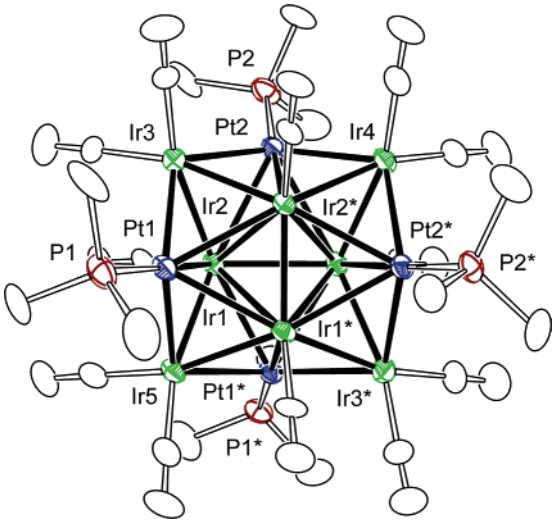

Figure 10. ORTEP diagram of the molecular structure of $Ir_8(CO)_{12}[Pt(PBu^t_3)]_4$ (**10**) showing 30% thermal ellipsoid probabilities. Methyl groups from the tri-*tert*-butyl phosphine ligands have been omitted for clarity.

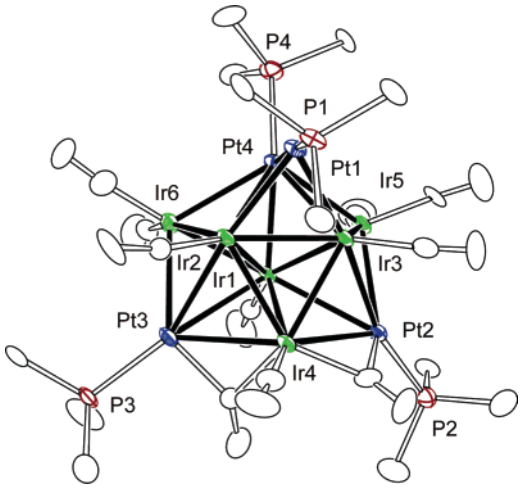

Figure 11. ORTEP diagram of the molecular structure of $Ir_6(CO)_{10}[Pt(PBu^t_3)]_4$ (**11**) showing 30% thermal ellipsoid probabilities. Methyl groups from the tri-*tert*-butyl phosphine ligands have been omitted for clarity.

10 also shows one resonance ($\delta = 92.5$ ppm) with appropriate one-bond coupling to platinum ($^1J_{Pt-P} = 4248$ Hz), indicating that all four phosphine groups are equivalent, as one would expect based on the overall D_{2d} molecular symmetry.

An ORTEP diagram of **11** is shown in Figure 11. Selected intramolecular distances and angles are listed in Table 4. Like that of **10**, the structure of **11** also contains a central $Ir_4(CO)_4$ pseudotetrahedron, but there are only two edge-bridging $Ir(CO)_2$ groups and four $Pt(PBu^t_3)$ groups. One of these, Pt(4), is bonded to five iridium atoms in an arrangement similar to those observed in **10**. Two platinums are bonded to four iridium atoms: three from the central $Ir_4(CO)_4$ pseudotetrahedron and one of the bridging $Ir(CO)_2$ groups. The fourth $Pt(PBu^t_3)$ group, Pt(1), is bonded only to two of the iridium atoms in the $Ir_4(CO)_4$ pseudotetrahedron and one of the $Pt(PBu^t_3)$ groups through a direct Pt−Pt bond, Pt(1)−Pt(4) = 2.6674(6) Å. The Ir−Ir bond distances in the central $Ir_4(CO)_4$ unit are similar to those observed for **9** and **10**. As with **10**, the bond distances between Ir(5) and Ir(6) and the central Ir_4 pseudotetrahedron are quite short, 2.5833(6)−2.6077(7) Å. Ir(1) is bonded to eight of the nine other metal atoms in the metal cluster. The distances of

Table 4. Selected Intramolecular Distances and Angles for Compounds **11** and **12**[a]

11		**12**	
	Bond Distances (Å)		
Ir(1)−Ir(2)	2.7106(6)	Ir(1)−Ir(2)	2.7093(3)
Ir(1)−Ir(3)	2.6911(6)	Ir(1)−Ir(3)	2.6977(3)
Ir(2)−Ir(6)	2.6077(7)	Ir(2)−Ir(6)	2.6072(3)
Ir(3)−Ir(5)	2.5833(6)	Ir(3)−Ir(5)	2.5939(3)
Pt(1)−Ir(2)	2.6231(6)	Pt(1)−Ir(2)	2.6589(3)
Pt(1)−Ir(3)	2.6158(7)	Pt(1)−Ir(3)	2.6255(3)
Pt(2)−Ir(1)	2.9241(7)	Pt(2)−Ir(1)	2.8997(3)
Pt(2)−Ir(4)	2.8544(6)	Pt(2)−Ir(4)	2.7532(3)
Pt(2)−Ir(5)	2.7983(8)	Pt(2)−Ir(5)	2.8369(4)
Pt(3)−Ir(1)	2.9020(6)	Pt(3)−Ir(1)	2.8826(3)
Pt(3)−Ir(4)	2.8289(7)	Pt(3)−Ir(4)	2.7457(4)
Pt(3)−Ir(6)	2.7359(7)	Pt(3)−Ir(6)	2.8140(3)
Pt(1)−Pt(4)	2.6674(6)	Pt(1)−Pt(4)	2.6703(3)
Pt(1)−P(1)	2.273(3)	Pt(1)−P(1)	2.261(2)
Pt(4)−P(4)	2.319(4)	Pt(4)−P(4)	2.335(2)
C−O (av)	1.15(2)	C−O (av)	1.15(2)
	Bond Angles (deg)		
P(1)−Pt(1)−Pt(4)	177.91(10)	P(1)−Pt(1)−Pt(4)	179.41(4)
P(4)−Pt(4)−Pt(1)	105.80(8)	P(4)−Pt(4)−Pt(1)	104.80(4)

[a] Estimated standard deviations in the least significant figure are given in parentheses.

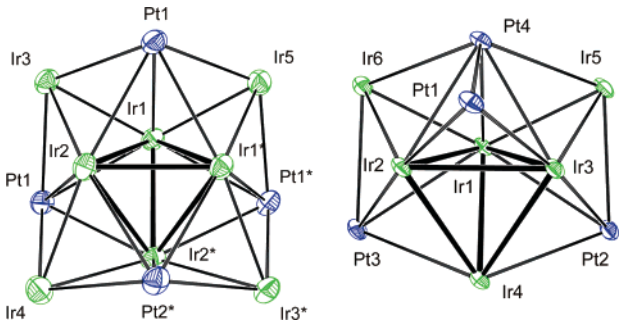

Figure 12. ORTEP diagrams of the metal frameworks of **10** and **11** showing 30% thermal ellipsoid probabilities. The interior Ir_4 tetrahedra are shown in bold.

Ir(1)−Pt(2) = 2.9241(7) Å and Ir(1)−Pt(3) = 2.9020(6) Å are slightly elongated. The distances of Pt(1)−Ir(2) = 2.6231(6) Å and Pt(1)−Ir(3) = 2.6158(7) Å are relatively short. The PBu^t_3 group bonded to Pt(1), Pt(1)−P(1) = 2.273(3) Å, is significantly displaced from its symmetric 3-fold position [e.g., Pt(4)−Pt(1)−P(1) = 177.91(10)°]. The ^{1}H NMR spectrum at room temperature shows two resonances at 0.93 and 1.61 ppm in a 2:1 ratio, as well as a broad resonance at 1.80 ppm. The broad resonance is most likely caused by the hindered rotations of the *tert*-butyl groups on P(1) due to steric interactions with the neighboring carbonyl groups on Ir(2) and Ir(3).[6c,15] When the temperature was increased to 100 °C, this signal sharpened, and the ^{1}H NMR spectrum showed three sharp resonances in a 2:1:1 ratio, as expected with appropriate couplings to the phosphorus atoms.

For comparison, ORTEP diagrams of the metal frameworks of compounds **10** and **11** are given in Figure 12. Both compounds have an interior $Ir_4(CO)_4$ tetrahedron (shown in bold) with at least three face-bridging $Pt(PBu^t_3)$ groups and two edge-bridging $Ir(CO)_4$ groups. Compound **10** can be generated from **11** by moving Pt(1) from the Ir(2)−Ir(3)−Pt(4) triangle to the Ir(2)−Ir(3)−Ir(4) triangle and subsequent addition of two $Ir(CO)_2$ groups. Attempts to achieve this conversion synthetically were unsuccessful.

(15) Rithner, C. D.; Bushweller, C. H. *J. Am. Chem. Soc.* **1985**, *107*, 7823. (b) Bushweller, C. H.; Brunelle, J. A. *J. Am. Chem. Soc.* **1973**, *95*, 5949.

Scheme 2

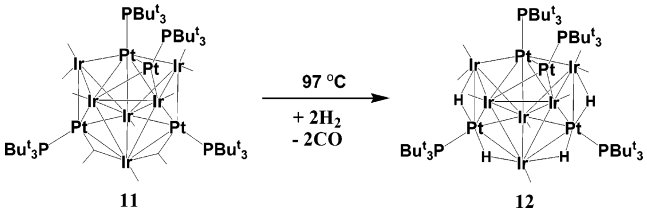

Reaction of 11 with H_2. Compound **11** reacted with hydrogen at 97 °C to give the new decanuclear compound $Ir_6(CO)_8[PtP(Bu^t_3)]_4(\mu\text{-}H)_4$ (**12**) in 45% yield (Scheme 2). Compound **12** was characterized by a combination of IR, ^1H and ^{31}P NMR, mass spectra, elemental, and single-crystal X-ray diffraction analyses. The ^1H NMR spectrum of **12** at −50 °C shows two hydride resonances of equal intensity at −10.30 and −14.98 ppm that both show one-bond coupling to platinum ($^1J_{Pt-H}$ = 709 and 763 Hz, respectively) and two-bond coupling to phosphorus ($^2J_{P-H}$ = 39 and 7 Hz, respectively). The proton−proton coupling was undoubtedly small and not observed as the angles of Ir(4)−Pt(2)−Ir(5) = 101.545(10)° and Ir(4)−Pt(3)−Ir(6) = 102.149(10)° are close to 90°. As the temperature is increased, the resonances slowly begin to broaden and move closer together. At 100 °C, the spectrum had not yet reached coalescence, and no further measurements at higher temperatures were taken. This is indicative of a dynamical averaging process where all hydrido ligands become equivalent. The mass spectrum of **12** indicated the presence of four hydrido ligands, so they must be present as two inequivalent pairs. This was confirmed by the low-temperature single-crystal X-ray diffraction analysis.

An ORTEP diagram of the molecular structure of **12** is shown in Figure 13. Selected intramolecular distances and angles are listed in Table 4. The Ir_6Pt_4 cluster of **12** is similar to that of **11**. The principal difference between **11** and **12** is that **12** contains two fewer carbonyl ligands than **11** and **12** has four hydrido ligands (**11** has no hydrido ligands). Two of these hydrido ligands, H(2) and H(3), have replaced the two bridging carbonyls in **11** across the Pt(2)−Ir(4) and Pt(3)−Ir(4) bonds. These substitutions cause a decrease in these two bond lengths from 2.8548(7) and 2.8292(7) Å, respectively (in **11**), to 2.7532(3) and 2.7457(4) Å, respectively (in **12**). While it is well established that bridging hydrido ligands generally cause increases in the length of the associated metal−metal bond, we have found previous examples that hydride bridges associated with $PtP(Bu^t_3)$ groups can cause significant shortening of the associated metal−metal bond.[16] Two additional hydrido ligands were found bridging the adjacent Pt(2)−Ir(5) and Pt(3)−Ir(6) bonds. In these two cases, the associated metal−metal bonds were increased in length from 2.7984(8) and 2.7355(8)Å, respectively (in **11**), to 2.8369(4) and 2.8140(3) Å, respectively (in **12**). All other bond distances in **12** are similar to those observed in **11**.

(16) Teller, R. G.; Bau, R. *Struct. Bonding* **1981**, *41*, 1.

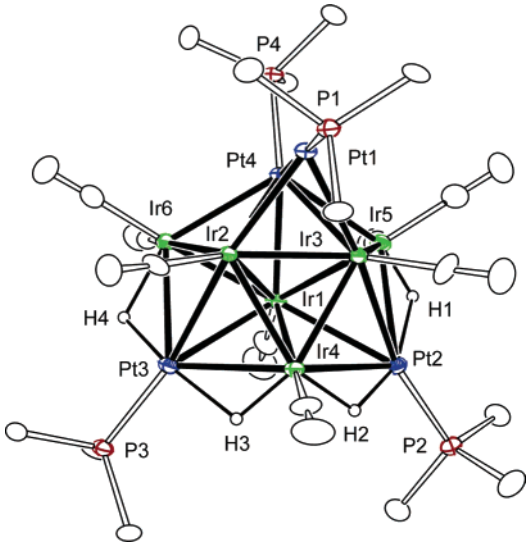

Figure 13. ORTEP diagram of the molecular structure of $Ir_6(\mu\text{-}H)_4(CO)_8[Pt(PBu^t_3)]_4$ (**12**) showing 60% thermal ellipsoid probabilities. Methyl groups from the tri-*tert*-butyl phosphine ligands have been omitted for clarity.

Concluding Remarks

This work further demonstrates the addition of $Pt(PBu^t_3)$ groups to metal−metal bonds. The reaction of $Pt(PBu^t_3)_2$ with $Ir_4(CO)_{12}$ at room temperature has given the adduct $Ir_4(CO)_{12}[Pt(PBu^t_3)]_2$ (**9**). The stability of **9** is derived from the cluster-bonding orbitals that are produced by Ir d-fragment orbitals, which have been stabilized by the CO π-acceptor, interacting with Pt d-orbitals, which have been destabilized by the phosphine σ-donor. The ligand bonding brings the relative energies of these fragment orbitals into coincidence such that proper symmetry combinations form delocalized cluster-bonding orbitals. At 110 °C, the reaction of $Pt(PBu^t_3)_2$ with $Ir_4(CO)_{12}$ gave two new high nuclearity clusters, $Ir_8(CO)_{12}[Pt(PBu^t_3)]_4$ (**10**) and $Ir_6(CO)_{10}[Pt(PBu^t_3)]_4$ (**11**). The latter compound reacted with hydrogen at 97 °C to yield $Ir_6(\mu\text{-}H)_4(CO)_8[Pt(PBu^t_3)]_4$, **12**. These compounds also seem to be active toward small organic molecules and should serve as excellent precursors to heterogeneous catalysts.

Acknowledgment. This research was supported by the Office of Basic Energy Sciences of the U.S. Department of Energy under Grant DE-FG02-00ER14980. We thank Strem for the donation of a sample of $Pt(PBu^t_3)_2$, and Dr. Perry J. Pellechia for assistance in recording NMR spectra. We also thank Dr. Mark D. Smith for collecting X-ray data at low temperature. The work at TAMU was supported by the National Science Foundation (CHE 98-00184), The Welch Foundation (A-0648), and Texas A&M University.

Supporting Information Available: CIF tables for the structural analyses of **9**−**12**. This material is available free of charge via the Internet at http://pubs.acs.org.

JA0443777